南京航空航天大学

论文集

（二〇〇七年）　第3期

航空宇航学院

（第3分册）

南京航空航天大学科技部编

二〇〇八年三月

航空宇航学院

第三分册

航空宇航学院2007年学术论文清单（0132）

序号	姓名	职称	单位	论文题目	刊物、会议名称	年、卷、期
1	徐焜 许希武	博士 教授	0132 0132	Meso-mechanical analysis of 3D braided composites based on a finite element model	Journal of Engineering and Applied Sciences	2007.02.10
2	徐焜 许希武	博士 教授	0132 0132	三维编织复合材料弹性性能数值预测及细观应力分析	复合材料学报	2007.24.03
3	徐焜 许希武	博士 教授	0132 0132	三维编织复合材料渐进损伤的非线性数值分析	力学学报	2007.39.03
4	徐焜 许希武 田静	博士 教授 硕士	0132 0132 0132	小编织角三维编织复合材料拉伸强度模型	航空学报	2007.28.02
5	郭树祥 许希武	博士 教授	0132 0132	钉载作用下多裂纹板的裂纹闭合接触问题	航空学报	2007.28.01
6	黄晶 许希武	博士 教授	0132 0132	飞机壁板结构击穿的数值模拟	兵器材料科学与工程	2007.30.02
7	李晨 许希武	博士 教授	0132 0132	缝合复合材料层板面内局部纤维弯曲模型及刚度预报	应用力学学报	2007.24.02
8	李晨 许希武	博士 教授	0132 0132	缝合复合材料层板面内局部纤维弯曲模型及剪切强度预报	固体力学学报	2007.28.03
9	张楠 许希武	博士 教授	0132 0132	飞机铝合金蒙皮战伤安全评定方法试验	西北大学学报	2007.37.03
10	张楠 许希武 潘庆军	博士 教授	0132 0132	战伤飞机损伤极限的非迭代解法	哈尔滨工业大学学报	2007.39.06
11	史治宇	教授	0132	Identification of linear time-varying dynamical systems using Hilbert transform and EMD method	Journal of Applied Mechanics	2007.74.00
12	史治宇	教授	0132	Subspace-Based Identification of Time-Varying System	2nd internationl conference of Experimental Vibration Analysis for Civil Engineering Structures	2007
13	史治宇	教授	0132	Subspace-Based Identification of Linear Time-Varying System	AIAA Journal	2007.45.08
14	陈文 史治宇	硕士 教授	0132 0132	模型修正技术在Msc.Patran中的应用	Msc.Software虚拟产品开发(VPD)中国用户大会	2007
15	李会娜 史治宇	硕士 教授	0132 0132	基于自由响应数据的时变系统物理参数识别	振动工程学报	2007.20.04
16	周储伟 张音旅	教授 硕士	0132 0132	含边界和损伤的纺织复合材料细胞元模型	南京航空航天大学学报	2007.39.01
17	周储伟 张音旅	教授 硕士	0132 0132	三维机织复合材料多尺度黏弹性分析	复合材料学报	2007.24.05
18	张斌 梁拥成 孙慧玉	讲师 讲师 副教授	0132 外校 0132	Structural phase transition and failure of nanographite sheets under high pressure: a molecular dynamics study.	Journal of Physics: Condensed Matter	2007.19.346224
19	张斌 梁拥成 孙慧玉	讲师 讲师 副教授	0132 外校 0132	Theoretical compressive strength of nanographite films at ultrahigh pressure.	庆祝中国力学学会成立50周年大会暨中国力学学会学术大会’2007(CCTAM2007会议文集)专题研讨会(微纳米力学)：214	2007
20	张斌 郭万林	讲师 教授	0132 高新院	Three-dimensional stress state around quarter-elliptical corner cracks in elastic plates subjected to uniform tension loading.	Engineering Fracture Mechanics	2007.74.03
21	王鑫伟 王新峰 史旭东	教授 博士 硕士	0132 0132 0132	Accurate Buckling Loads of Thin Rectangular Plates under Parabolic Edge Compressions by Differential Quadrature Method	International Journal of Mechanical Sciences	2007.49.00

序号	姓名	职称	单位	论文题目	刊物、会议名称	年、卷、期
22	王鑫伟	教授	0132	Nonlinear Stability Analysis of Thin Doubly Curved Orthotropic Shallow Shells by the Differential Quadrature Method	Computers Methods in Applied Mechanics and Engineering	2007.196.00
23	龚俊杰 王鑫伟 王新峰	博士 教授 博士	0132 0132 0132	Study on self-adaptive trigger mechanism of composite tubes	World Forum on Smart Materials & Smart Structures SMSST' 07	2007
24	龚俊杰 王鑫伟	博士 教授	0132 0132	复合材料波纹梁盒段耐撞性的数值模拟	应用力学学报	2007.24.01
25	顾建祖 王鑫伟 骆英 龚仁荣	博士 教授 教授 硕士	0132 0132 外校 外校	正交异性压电传感器在结构健康诊断中的应用	振动工程学报	2007.20.04
26	黄再兴 P Thomson Dhenlin Di	教授 教授 博士	0132 外单位 外单位	lattice contractions of nanoparticle due to the surface tension: A model of elasticity	Journal of physics and chemistry of solids	2007.68.04
27	周丽 袁福国	教授 教授	0132 0132	A pre-stack migration method for damage identification in composite structures	Journal of Smart Structures and Systems	2007.03.04
28	周丽 吴新亚 杨振南	教授 硕士生 教授	0132 0132 0132	Shake table experimental verification for a structural damage identification technique	Proceedings of World Forum on Smart Materials and Smart Structures Technology	2007
29	严刚 周丽	博士生 教授	0132 0132	Identification of impact load for composites using genetic algorithms	Proceedings of 6th International Workshop on Structural Health Monitoring	2007.00.01
30	严刚 周丽	博士生 教授	0132 0132	基于Lamb波的复合材料结构损伤成像研究	仪器仪表学报	2007.28.04
31	严刚 周丽	博士生 教授	0132 0132	应用遗传算法和散射Lamb波的板结构损伤识别	振动工程学报	2007.20.03
32	严刚 周丽 孟伟杰	博士生 教授 硕士生	0132 0132	基于Lamb波与时频分析的复合材料结构损伤监测和识别	南京航空航天大学学报	2007.39.03
33	胡家亮 周丽	硕士生 教授	0132 0132	Semi-active flutter control of a high-aspect-ratio wing using multiple MR dampers	Sensors and Smart Structures Technologies for Civil, Mechanical, and Aerospace Systems, Proceedings of SPIE	2007.6529
34	李春雷 周丽 袁福国	硕士生 教授 教授	0132 0132 0132	Localization of damage and restoration of dynamic characteristics using distributed control	Sensors and Smart Structures Technologies for Civil, Mechanical, and Aerospace Systems, Proceedings of SPIE	2007.6529
35	吴新亚 周丽	硕士生 教授	0132 0132	基于有限范围自适应卡尔曼滤波的结构损伤识别方法	振动工程学报	2007.20.04
36	杨雅洁 周丽	硕士生 教授	0132 0132	用于板结构损伤检测的磁致伸缩传感器	传感器与微系统	2007.26.05
37	杨雅洁 周丽 袁福国	硕士生 教授 教授	0132 0132 0132	A magnetostrictive sensor for structural health monitoring in a non-ferromagnetic plate	Proceedings of World Forum on Smart Materials and Smart Structures Technology	2007.05
38	周光明	教授	0132	细编穿刺3D碳/碳复合材料双向拉伸实验研究	南京理工大学学报	2007.31.03
39	周光明	教授	0132	整体冲破式复合材料薄膜盖的设计与试验研究	宇航学报	2007.28.03
40	周光明	教授	0132	整体中空夹层复合材料力学性能的实验研究	南京航空航天大学学报	2007.39.01
41	黄佩珍	副教授	0132	谈如何适应弹性力学课的教学岗位	鞍山师范学院学报	2007.09.02
42	李志刚 黄佩珍 王远鹏	硕士 副教授	0132 0132 0132	同相位裂面形貌扰动对损伤微裂纹演化影响的数值分析	第三届江苏省固体力学学术年会	2007

序号	姓名	职称	单位	论文题目	刊物、会议名称	年、卷、期
43	孙慧玉	副教授	0132	美国高等教育的一些鲜明特点及其启示	黑龙江教育（高教研究与评估）	2007.00.12
44	孙慧玉	副教授	0132	三维纺织复合材料的弹性分析	大型飞机关键技术高层论坛暨中国航空学会2007年学术年会	2007
45	王新峰 王鑫伟 周光明 周储伟	讲师 教授 教授 教授	0132 0132 0132 0132	Multi-scale Analyses of 3D Woven Composite Based On periodicity boundary conditions	Journal of Composite Materials	2007.41.14
46	王新峰 王鑫伟 周光明 周储伟	讲师 教授 教授 教授	0132 0132 0132 0132	Multi-scale Analyses of Damage Evolution in Plain Woven Composites	Journal Engineering and Applide Science	2007.02.02
47	王新峰 周光明 王鑫伟	讲师 教授 教授	0132 0132 0132	平面机织复合材料的压缩损伤	材料科学与工程学报	2007.25.05
48	王新峰 周光明 王鑫伟 周储伟	讲师 教授 教授 教授	0132 0132 0132 0132	平面机织复合材料在剪切载荷下损伤刚度折减分析	宇航学报	2007.28.05

航空宇航学院2007年学术论文清单（0133）

序号	姓名	职称	单位	论文题目	刊物、会议名称	年、卷、期
1	胡明敏 张明 罗艳丽 方义庆	教授 副教授 硕士 硕士	0133 0133 0133 0133	应变倍增器研制与应用	实验力学	2007.22.01
2	胡明敏 张明 罗艳丽 李训涛	教授 副教授 硕士 硕士	0133 0133 0133 0133	桥梁疲劳监测传感器设计	传感器与微系统	2007.26.04
3	虞伟建 王妮 张彦	副教授 高工 技师	0133 0133 0133	槽型截面悬臂梁弯曲实验设计	实验技术与管理	2007.24.10
4	虞伟建 王妮 张彦	副教授 高工 技师	0133 0133 0133	大型飞机起落架光弹性试验模型制造	中国航空学会2007年学术会议	2007
5	刘荣梅 梁大开 王妮 张彦	讲师 教授 高工 技师	0133 0134 0134 0134	光纤拉伸试验机的设计研究	仪器仪表学报	2007.28.04
6	刘荣梅 梁大开 王妮 张彦	讲师 教授 高工 技师	0133 0134 0134 0134	光纤力学性能的试验研究	实验力学	2007.22.01
7	王开福 A.K.Tieu 高明慧	教授 教授 高工	0133 外校 062	Measurement of curvature distribution using digital speckle three-shearing aperture interferometry	Optics & Laser Technology	2007.39.05
8	宋凡峰 王开福 郑　蓝	硕士 教授 研究生	0133 0133 0133	电子散斑相位检测的滤波方法研究	激光杂志	2007.28.03

Journal of Engineering and Applied Sciences 2 (10): 1553-1562, 2007
ISSN: 1816-949X

Meso-Mechanical Analysis of 3D Braided Composites Based on a Finite Element Model

Xu Kun and Xu Xiwu
College of Aerospace Engineering, Nanjing University of Aeronautics and Astronautics,
Nanjing 210016, People's Republic of China

Abstract: As for 3D 4-directional rectangular braided composites, a 3-Dimensional (3D) Finite Element Model (FEM) based on a Representative Volume Element (RVE) is established under the periodical displacement boundary conditions, which truly simulates the spatial configuration of the braiding yarns. The FE software ABAQUS is adopted to study the mechanical properties of the composites, including the effective elastic properties and the meso-scale mechanical behaviors. The effects of the braiding angle and the fiber-volume fraction on the engineering elastic constants have been investigated in detail. The predicted effective elastic properties are in good agreement with the available experimental data, demonstrating the applicability of the FEM. By analyzing the stress distribution and deformation of the model, it is proved that the RVE-based FEM can obtain reasonable stress field and successfully represent the meso-scale mechanical behaviors of 3D braided composites containing periodical structures.

Key words: Braided composites, finite element model, effective elastic properties, stress distribution, unit cell

INTRODUCTION

Three-Dimensional (3D) braided composites have been attractive for industrial applications because of their excellent mechanical performances, such as better out-of plane stiffness, strength and high impact resistance, etc, compared with the fiber-reinforced laminated composites. However, due to their complicated architectures and anisotropic nature, it is difficult to predict the mechanical properties of 3D braided composites.

To make full use of 3D braided composites, many models have been developed to analyze the microstructure (Li *et al*., 1990; Du and Ko, 1993; Wang and Wang, 1994; Pandey and Hahn, 1996; Chen *et al*., 1999) and the mechanical properties (Ma *et al*., 1984, 1986; Sun and Sun, 2004; Sun and Qiao, 1997; Gu, 2004; Lei *et al*., 1992; Sun *et al*., 2003; Zeng *et al*., 2004; Tang and Postle, 2002; Chen *et al*., 1999; Yu and Cui, 2007). Ma *et al*. (1984, 1986) studied the effective elastic properties of 3D braided composites by using the 'Fiber interlock model' based on the maximum strain energy principle and the 'Fiber inclination model' based on the modified laminate theory. Wang and Wang adopted a mixed volume averaging technique to predict the mechanical properties of 3D braided composites. Sun and Sun (2004) reported a volume-average-compliance method to calculate the elastic constants. Sun and Qiao (1997) studied the tensile strength based on the modified classical laminate theory. Gu (2004) presented an analytical model to predict the uniaxial tensile strength based on the strain energy conservation law. Lei *et al*. (1992) adopted a 3D truss finite element technique to analyze the mechanical properties of 3D braided composites. Recently, two new prediction models based on finite element procedures (Sun *et al*., 2003; Zeng *et al*., 2001) were developed to evaluate the elastic performance of 3D braided composites. Tang and Postle (2002) analyzed the nonlinear deformation of 3D braided composites by the finite element method. Chen *et al*. (1999) proposed a finite multiphase element method to predict the effective elastic properties. Yu and Cui (2007) developed a two-scale method to predict the mechanics parameters of 3D braided composites.

Although these analytical and computational models have contributed to an enhanced understanding of the mechanical properties of 3D braided composites, the models have their own limitations. For example, simple architectures considered in the analytical models (Ma *et al*., 1984, 1986; Sun and Sun, 2004; Sun and Qiao, 1997) have great difference with the truly geometrical microstructure of 3D braided composites. As the analytical models based on the laminate theory have inherent limitations in geometrical modeling, they are mainly devoted to predicting the global stiffness properties of 3D braided composites. Further, the computational models based on finite element methods

Corresponding Author: Xu Kun, College of Aerospace Engineering, Nanjing University of Aeronautics and Astronautics, Nanjing 210016, People's Republic of China

(Lei *et al.*, 1992; Sun *et al.*, 2003; Zeng *et al.*, 2004; Tang and Postle, 2002) also considered the architectures of the composites to be too simplified and the uniform strain boundary conditions were applied in the periodical unit cell model (Chen *et al.*, 1999), which made it difficult to obtain an accurate local stress distribution of 3D braided composites.

In order to predict the mechanical properties of 3D braided composites, it is necessary to establish a model for obtaining the accurate stress distribution of 3D braided composites. However, there are few literatures on predicting the local stress distribution and deformation of 3D braided composites, which is important to accurately predict their mechanical properties. Compared with the analytical models based on the laminate theory, 3D meso-mechanical finite element methods can contribute to truly model the microstructure of 3D braided composites. The main objective of the present work is to develop a new 3D finite element model for obtaining the stress distribution and effective elastic properties of 3D braided composites. The model has taken into account the periodical structure of the composites and the interaction between the braiding yarns. The periodical displacement boundary conditions have been applied in the model. In order to fully exploit the potential of 3D braided composites, the effect of the braiding angle and the fiber-volume fraction on the mechanical properties is analyzed in detail. The predicted effective elastic properties are in good agreement with the available experimental data, demonstrating the applicability of the meso-mechanical FEM. By analyzing the stress distribution and deformation of the model, some conclusions are drawn herein.

MICROSTRUCTURE ANALYSIS AND UNIT CELL MODEL

Although a few representative unit cell geometrical models (Li *et al.*, 1990; Du and Ko, 1993; Wang and Way, 1994; Pandey and Hahn, 1996; Chen *et al.*, 1999) have been proposed to describe the microstructure of 3D braided composites, some assumptions of these models are apparently unreasonable or too simple. It makes some vital architecture features of the yarn configuration inconsistent with the true microstructure of 3D braided composites. For example, 3D braided composites are composed of the complex fiber-bundle geometry and the matrix pockets. In order to consider the mutual squeeze of the yarns, the cross-section shape of the yarn has usually been supposed to be elliptical. The assumption makes the configuration of the yarns apparently different with the experimental phenomena observed experimentally (Chen *et al.*, 1999) which showed that the yarns contacted with each other by sharing a plane due to their mutual squeeze. This important microstructure feature should not be neglected in the geometrical modeling, which greatly influences the stress distribution of 3D braided composites.

In order to perform the analysis of mechanical performances of 3D braided composites successfully, it is important to establish a reasonable microstructure geometrical model which can describe the spatial configuration of the yarns effectively. According to the movement of the yarn carriers on the braiding machine bed and experimental observation (Chen *et al.*, 1999) the microstructure of 3D 4-directional braided composites produced by the four-step 1×1 braiding procedure has been investigated in detail.

To ensure consistent and uniform fabric structure, suppose the braiding procedure keep relatively steady, at last in a specified length of braiding. According to the movements of carriers, 3D 4-directional braided composites can be regarded to be made of an infinite of two kinds of repeated sub-cells, A and B. Figure 1 schematically shows the distribution of sub-cell A and sub-cell B in the cross-section of rectangular specimen. As shown in Fig. 1, sub-cell A and sub-cell B are constructed, respectively, based on two braiding yarns in the cross directions. The difference between sub-cell A and sub-cell B is the spatial directions of the braiding yarns. It is noteworthy that sub-cell A and sub-cell B marked with the dash lines distribute alternately every half of a pitch length h in the braiding direction of the z axis, as shown in Fig. 2.

Due to the complicated microstructure of 3D braided materials, it makes unfeasible to undertake a full micromechanical simulation aiming at a whole structure. Instead, Representative Volume Element (RVE)-based approach can be used to analyze the mechanical properties in the macro-meso scales. Considering the periodical feature of sub-cell distribution, a unit cell that is the smallest periodical RVE is selected as shown in Fig. 1. According to the unit cell partition scheme, all the unit cells are oriented in the same reference frame as the specimen, which is quite favorable for the analysis of the mechanical properties. Figure 2 shows the topological relation of the main yarns in a parallelepiped unit cell. γ is the angle between the central axis of the braiding yarn and the z-axis. The relationship between the angle γ and the surface braiding angle α, is defined as

$$\tan\gamma = \sqrt{2}\tan\alpha \quad (1)$$

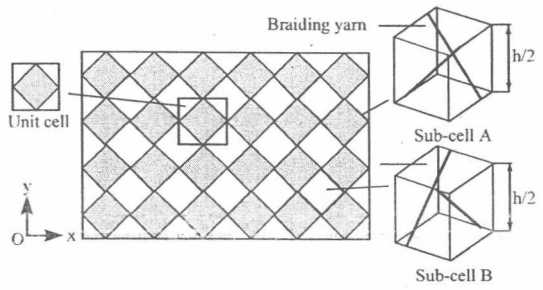

Fig. 1: Distribution of unit cells on the cross-section of rectangular specimen

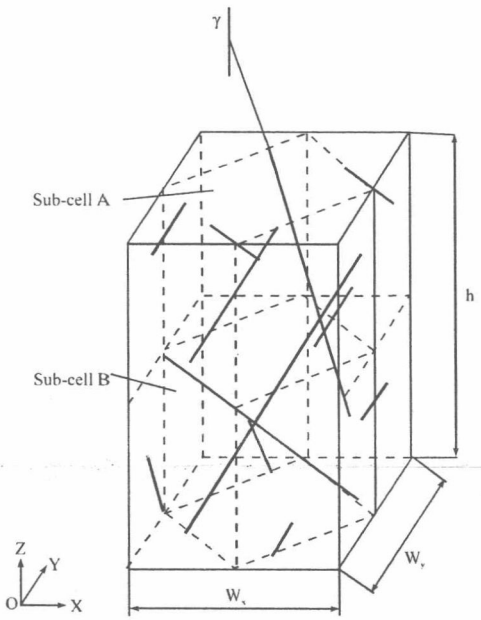

Fig. 2: Topological relation of the main yarns in the unit

The solid unit cell model of 3D 4-directional braided composites is shown in Fig. 3. All the yarns used in the braided performs are assumed to have the same constituent material, size and flexibility. Considering the mutual squeezing of the yarns, the cross-section shape of the braiding yarn perpendicular to the central axis is assumed to be octagonal and the octagon contains an inscribed ellipse with major and minor radii, a and b, respectively, which is shown in Fig. 4.

The width and the pitch length of the unit cell are, respectively

$$W_x = W_y = 4\sqrt{2}b \tag{2}$$

and

$$h = \frac{8b}{\tan\gamma} \tag{3}$$

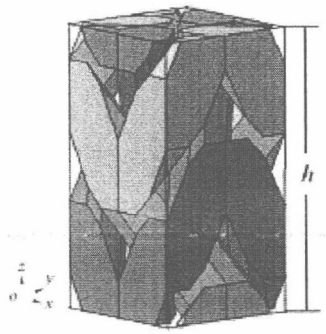

Fig. 3: Yarn configuration of the solid unit cell

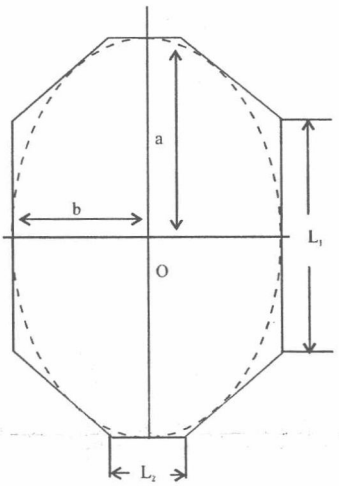

Fig. 4: Cross-section shape of yarn

According to the tangent relationship of the elliptical-cylinders of the braiding yarns, the relationship between the major and minor radii of the inscribed ellipse, a and b, can be obtained:

$$a = \sqrt{3}b\cos\gamma \tag{4}$$

The lengths of L_1 and L_2 in Fig. 4, are given by:

$$L_1 = 2\left[\sqrt{b^2\cot^2\gamma + \frac{a^2}{\sin^2\gamma}} - b\cot\gamma\right]\sin\gamma \tag{5}$$

$$L_2 = 2\left[\sqrt{b^2\cot^2\gamma + \frac{a^2}{\sin^2\gamma}}\right]\sin\gamma \tag{6}$$

As the idealized braided composites considered herein are assumed to be made of the repeated unit cells, the fiber volume fraction of 3D braided composites can be determined by the following expression:

$$V_f = \frac{V_y}{V_u}\varphi \tag{7}$$

Where, V_y is the volume of all the yarns in the unit cell, V_u is the volume of the whole unit cell and φ is the fiber volume fraction of the yarn.

The 3D solid unit cell can be established by using the CAD/CAM software CATIA P3 V5R14.

FINITE ELEMENT MODEL

The RVE-based meso-mechanical FEM mainly consists of three parts: The periodical boundary conditions and finite element meshing, the constitutive relations of components and the definition of the effective elastic properties. The details of the finite element model are presented in the subsections.

Periodical displacement boundary conditions and finite element meshing: Since the analysis is based on the RVE, the periodical boundary conditions should be applied in the model in order to obtain a reasonable stress distribution. Two continuities must be satisfied at the boundary surfaces of the neighboring cubic RVEs. The first is that the displacements must be continuous, and the second is that the traction distribution at the opposite parallel boundaries of the RVE must be uniform. Therefore, the unified periodical displacement boundary conditions suitable for the RVE proposed by Xia *et al.* (2003) were employed in the model. These general formulas of the boundary conditions are given as follows:

$$u_i = \bar{\varepsilon}_{ik} x_k + u_i^* \tag{8}$$

$$u_i^{j+} = \bar{\varepsilon}_{ik} x_k^{j+} + u_i^* \tag{9}$$

$$u_i^{j-} = \bar{\varepsilon}_{ik} x_k^{j-} + u_i^* \tag{10}$$

$$u_i^{j+} - u_i^{j-} = \bar{\varepsilon}_{ik}(x_k^{j+} - x_k^{j-}) = \bar{\varepsilon}_{ik}\Delta x_k^j \tag{11}$$

In Eq. 8, $\bar{\varepsilon}_{ik}$ is the global average strain tensor of the periodical structure, μ^*_i is the periodic part of the displacement components on the boundary surfaces and it is generally unknown. For a cubic RVE as shown in Fig. 4, the displacements on a pair of opposite boundary surfaces (with their normals along the X_j axis) are expressed as in Eq. 9 and 10, in which the index "j+" means along the positive X_j direction and "j-" means along the negative X_j direction. The difference between Eq. 9 and 10 is given in Eq. 11. Since Δ^j_k are constants for each pair of the parallel boundary surfaces, with specified $\bar{\varepsilon}_{ik}$, the right side of Eq. 11 become constants.

It can be seen that Eq. 11 does not contain the periodic part of the displacement. It becomes easier to apply the nodal displacement constraint equations in the finite element procedure, instead of giving Eq. 8 directly as the boundary conditions. In order to apply the constraint Eq. 11 in the FEM, the same meshing at each two paired boundary surfaces of the RVE should be produced.

Due to the complexity of the microstructure the 3D solid tetrahedron elements were applied to mesh the whole model, as shown in Fig. 5. The model is composed of the straight yarns in various directions and the matrix pocket from Fig. 5. It is assumed that the perfect bonding exists between the yarns and the resin matrix pocket. Uniform meshes had been made to satisfy the continuities of stress and displacement on the interfaces of the constitutive materials, including the interfaces of the yarns in different directions and the interfaces between the yarns and the resin matrix pocket.

Constitutive relations of components: As shown in Fig. 5, two "types" of materials are contained in the model. They are the yarns and the resin matrix pocket, respectively. The yarns can generally be regarded as the unidirectional fiber-reinforced composites in the material coordinates systems. The principal direction 1 of the material coordinates systems for a yarn is defined to be paralleled with the fiber direction. The yarns and the resin matrix pocket are assumed to be transversely isotropic and isotropic, respectively. Both of them are believed to be linearly elastic in the model. The engineering elastic constants of the yarn can be calculated by the famous micromechanics formulae proposed by Chamis (1989):

$$\begin{aligned}
&E_1 = \varphi E_{f1} + (1-\varphi)E_m,\\
&E_2 = E_3 = \frac{E_m}{1-\sqrt{\varphi}(1-E_m/E_{f2})},\\
&G_{12} = G_{31} = \frac{G_m}{1-\sqrt{\varphi}(1-G_m/G_{f12})},\\
&G_{23} = \frac{G_m}{1-\sqrt{\varphi}(1-G_m/G_{f23})},\\
&\nu_{12} = \nu_{13} = \varphi\cdot\nu_{f12} + (1-\varphi)\nu_m,\\
&\nu_{23} = \frac{E_2}{2G_{23}} - 1.
\end{aligned} \tag{12}$$

Where, φ is the fiber volume fraction of the yarn, E_{f1} is the Young's elastic modulus of the fiber in principle axis *1*, E_{f2} is the Young's elastic modulus of the fiber in

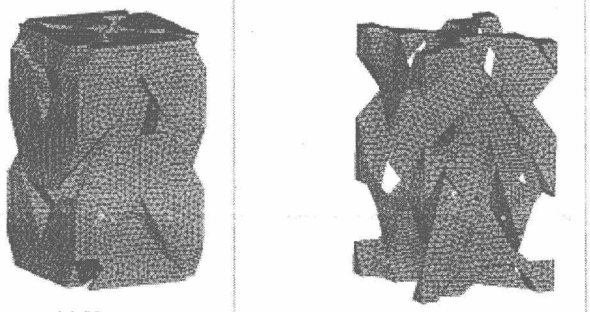

(a) Yarns (b) Resin matrix pocket

Fig. 5: Finite element mesh of the model

principle axis 2, G_{f12} is the longitudinal shear modulus of the fiber, G_{f23} is the transverse shear modulus of the fiber, v_{f12} is the primary Poisson's ratio of the fiber, E_m, V_m, and $G_m(G_m = E_m/2(1 + v_m))$ represent the Young's elastic modulus, Poisson's ratio and shear modulus of the matrix, respectively.

Effective elastic properties: To obtain the effective elastic properties of 3D 4-directional braided composites, a homogenization approach is employed in this study by considering the heterogeneous composites in the micro-scale to be a homogeneous material in the macro-scale. Given the periodic cubic RVE, the global strain-global stress relation can be written as

$$\bar{\varepsilon}_i = S_{ij}\bar{\sigma}_j \tag{13}$$

Where, S_{ij} is the effective compliance matrix. Assuming a set of the global strain, $\bar{\varepsilon}_{ik}$ and applying the periodic boundary conditions in the form of Eq. 11 in the FEM analysis, we can obtain a unique stress distribution of the RVE. Then the global stress, $\bar{\sigma}_{ik}$, corresponding to this set of global strains can be obtained by

$$\bar{\sigma}_{ij} = \frac{1}{V}\int_V \sigma_{ij}\, dV \tag{14}$$

In the 3D case applying this set of $\bar{\varepsilon}_{ik}$ (six components), six equations thus can be obtained. For a general case where there is no orthotropic axis of symmetry of the material, the application of four linearly independent sets of the global strains $\bar{\varepsilon}_{ik}$ will have sufficient equations to determine 21 independent material constants of the compliance matrix S_{ij} (Xia *et al.*, 2003).

As the effective compliance matrix S_{ij} is one of the inherent properties for 3D braided materials with the decided microstructure and component materials, the calculation of its value has on relation with the boundary conditions applied on the RVE. To avoid the trouble of solving the equations, six sets of global strains were applied in the FE analysis of RVE. Six sets of loading case of periodical displacement boundary conditions are shown in Table 1.

Table 1: Loading cases of periodical displacement boundary conditions

k	$\bar{\varepsilon}_x$	$\bar{\varepsilon}_y$	$\bar{\varepsilon}_z$	$\bar{\gamma}_{yz}$	$\bar{\gamma}_{zx}$	$\bar{\gamma}_{xy}$
1	0.01	0	0	0	0	0
2	0	0.01	0	0	0	0
3	0	0	0.01	0	0	0
4	0	0	0	0.02	0	0
5	0	0	0	0	0.02	0
6	0	0	0	0	0	0.02

By prescribing the six sets of the global strains, $\bar{\varepsilon}_{ij}^{k}$ (k = 1,2..6), the corresponding global stress $\bar{\sigma}_{ij}^{k}$ can be calculated by Eq. 14. Then the following equations can be obtained

$$\left\{\bar{\varepsilon}_{ij}^{1}, \bar{\varepsilon}_{ij}^{2}, \ldots, \bar{\varepsilon}_{ij}^{5}, \bar{\varepsilon}_{ij}^{6}\right\} = S_{ij}\left\{\bar{\sigma}_{ij}^{1}, \bar{\sigma}_{ij}^{2}, \ldots, \bar{\sigma}_{ij}^{5}, \bar{\sigma}_{ij}^{6}\right\} \tag{15}$$

It is easy to obtain the effective compliance matrix S_{ij} through

$$S_{ij} = \left\{\bar{\varepsilon}_{ij}^{1}, \bar{\varepsilon}_{ij}^{2}, \ldots, \bar{\varepsilon}_{ij}^{5}, \bar{\varepsilon}_{ij}^{6}\right\}\left\{\bar{\sigma}_{ij}^{1}, \bar{\sigma}_{ij}^{2}, \ldots, \bar{\sigma}_{ij}^{5}, \bar{\sigma}_{ij}^{6}\right\}^{-1} \tag{16}$$

RESULTS AND DISCUSSION

Comparison of effective elastic properties with experimental results: In order to verify the applicability of the FEM based on the software ABAQUS, three examples with typical braiding angles are selected from the available experiments studied by Chen *et al.* (1999). All the analyses reported herein were done for the 3D 4-directional braided composites by the 4-step 1×1 rectangular braiding procedures. The elastic properties of

Table 2: Mechanical properties of component materials

Materials	E_{f1} (GPa)	E_{f2} (GPa)	G_{f12} (GPa)	G_{f23} (GPa)	v_{f12}	v_m
Carbon fiber T300	230	40	24	14.3	0.25	
Epoxy resin	3.5					0.35

Table 3: Braiding parameters of specimens and structural parameters of unit cell model

	Braiding parameters of specimens			Structural parameters of unit cell model					
No.	Dimensions (mm)	α(°)	V_f(%)	γ(°)	a(mm)	b(mm)	φ(%)	$W_x = W_y$ (mm)	h (mm)
1	20×6×250	19.0	46.6	26.0	0.599	0.385	57.8	2.175	6.317
2	20×6×250	30.0	47.2	39.2	0.542	0.404	60.7	2.286	3.950
3	20×6×250	37.0	47.1	46.8	0.503	0.425	62.3	2.402	3.188

the component materials, including 12K T300 carbon fiber and TDE-85 epoxy resin, are listed in Table 2. According to the braiding process parameters of three specimens from Chen *et al.* (1999) the main microstructure parameters of unit cell models used in the calculation is shown in Table 3.

According to the meshing scheme of the FEM, adaptive finite element meshes were used to keep element size small in the edges of the matrix pocket. In the study, the FEM for specimen No.1 consists of 9854 nodes and 49030 tetrahedron elements. The FEM for specimen No.2 consists of 17462 nodes and 88700 tetrahedron elements, the FEM for specimen No.3 consists of 15298 nodes and 78518 tetrahedron elements. It is noted that relatively fine meshing size is required in order to obtain more accurate stress distribution, especially near the boundaries of the RVE. However, if only the global stiffness is concerned, relative coarse meshing size can still provide satisfactory results (Xia *et al.*, 2006). The meshing size of the models in this study is sufficient to guarantee the convergence of the solutions.

The effective elastic properties of 3D braided composites are first calculated by the FEM and the calculated stiffness properties are compared with Chen *et al.* (1999). The effective compliance matrix S_{ij} for specimen No.1, 2 and 3 are given, respectively, as follows:

$$S_{ij}=\begin{bmatrix} 0.1208 & -0.0425 & -0.0126 & 0 & 0 & 0 \\ -0.0425 & 0.1208 & -0.0126 & 0 & 0 & 0 \\ -0.0126 & -0.0126 & 0.0182 & 0 & 0 & 0 \\ 0 & 0 & 0 & 0.0965 & 0 & 0 \\ 0 & 0 & 0 & 0 & 0.0965 & 0 \\ 0 & 0 & 0 & 0 & 0 & 0.2535 \end{bmatrix} \times 10^{-3}\ 1/\text{MPa},$$

$$S_{ij}=\begin{bmatrix} 0.1173 & -0.0352 & -0.0284 & 0 & 0 & 0 \\ -0.0352 & 0.1173 & -0.0284 & 0 & 0 & 0 \\ -0.0284 & -0.0284 & 0.0415 & 0 & 0 & 0 \\ 0 & 0 & 0 & 0.0676 & 0 & 0 \\ 0 & 0 & 0 & 0 & 0.0676 & 0 \\ 0 & 0 & 0 & 0 & 0 & 0.1412 \end{bmatrix} \times 10^{-3}\ 1/\text{MPa}$$

and

$$S_{ij}=\begin{bmatrix} 0.1110 & -0.0340 & -0.0388 & 0 & 0 & 0 \\ -0.0340 & 0.1110 & -0.0388 & 0 & 0 & 0 \\ -0.0388 & -0.0388 & 0.0624 & 0 & 0 & 0 \\ 0 & 0 & 0 & 0.0642 & 0 & 0 \\ 0 & 0 & 0 & 0 & 0.0642 & 0 \\ 0 & 0 & 0 & 0 & 0 & 0.0973 \end{bmatrix} \times 10^{-3}\ 1/\text{MPa}$$

It is found that 3D 4-directional braided composites can be considered to be transversely isotropic materials in the macro-scale under small deformation assumption. According to the relationship between the engineering elastic constants and the compliance matrix S_{ij}, the engineering elastic constants of 3D 4-directional braided composites, including nine independent elastic constants, can be calculated by

$$\begin{cases} E_x = \dfrac{1}{S_{11}},\quad E_y = \dfrac{1}{S_{22}},\quad E_z = \dfrac{1}{S_{33}} \\ \mu_{xy} = -\dfrac{S_{12}}{S_{22}},\ \mu_{xz} = -\dfrac{S_{13}}{S_{33}},\ \mu_{yz} = -\dfrac{S_{23}}{S_{33}} \\ G_{yz} = \dfrac{1}{S_{44}},\quad G_{xz} = \dfrac{1}{S_{55}},\quad G_{xy} = \dfrac{1}{S_{66}} \end{cases} \tag{17}$$

Table 4 gives the predicted and measured elastic constants of 3D braided composite. There is a good agreement between the measured and predicted axial tensile modulus for all the three samples studied. The predicted Poisson' ratios are basically agreed with the measured values. The results indicate that the proposed FEM can be used to calculate the global elastic properties, demonstrating the applicability of the meso-mechanical FEM.

Deformation of unit cell and distribution of stress: For 3D 4-directional braided composites with periodical structures, RVE-based finite element model can also be used to calculate the mechanical properties in the meso-scale, such as the deformation of the model, distribution

Table 4: Comparison of the effective elastic constants predicted by the model and experimental data

	No.1		No.2		No.3	
Elastic constants	Experiment	Predicted	Experiment	Predicted	Experiment	Predicted
E_x/GPa		8.28		8.52		9.01
E_y/GPa		8.28		8.52		9.01
E_z/GPa	58.74	54.85	27.60	24.12	18.05	16.03
G_{xz}/GPa		10.36		14.80		15.57
G_{yz}/GPa		10.36		14.80		15.57
G_{xy}/GPa		3.95		7.08		10.27
V_{xz}	0.72	0.69	0.78	0.68	0.80	0.62
V_{yx}	0.69	0.69	1.00	0.68	0.72	0.62
V_{xy}		0.35		0.30		0.31

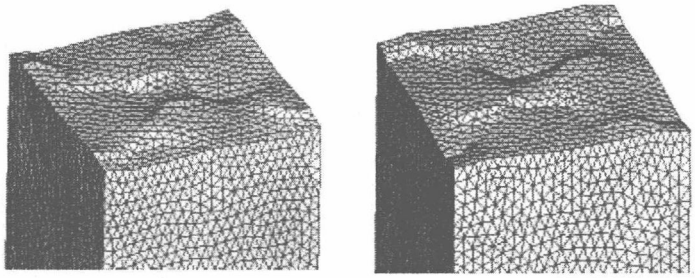

(a) Deformation of positive surface vertical to *z* axis

(b) Deformation of negative surface vertical to *z* axis

Fig. 6: Surface deformation of the model under loading case 3

of stress and stress concentration, etc. To demonstrate the application, the FEM of specimen No.2 subjected to typical loading cases is chosen to show the meso-mechanical behavior of 3D 4-directional braided composites.

Figure 6 shows the deformation of two parallel boundary surfaces vertical to the z axis of the model subjected to loading case 3, k = 3. Under such loading case, $\bar{\varepsilon}_a$ equals to 0.01 and all the other 5 effective average strains equal to zero. From Fig. 6, the two opposite boundary surfaces do not remain plane any more and are warped after the deformation (the magnified factor of the deformation is 100 times). The warped deformation occurs simultaneously at the other two sets of opposite boundary surfaces of unit cell, but the warped extent is relatively weak. The reason resulted in the phenomena is that the unit cell model of 3D 4-directional braided composites does not have the symmetries of geometrical structure and physical properties.

Figure 7 shows the deformation of the model subjected to loading case 6, k = 6. Under such loading case, $\bar{\gamma}_a$ equals to 0.02 and all the other five effective average strains equal to zero. From Fig. 7, the set of opposite boundary surfaces vertical to the x axis, respectively, do not remain plane after deformation and the warped deformation has occurred (the magnified factor of the deformation is 50 times). The same warped deformation occurs simultaneously at the opposite boundary surfaces vertical to the y axis. However, the warped deformation extent at the opposite boundary surfaces vertical to the z axis is relatively weak. From Fig. 6 and 7, the FEM based on the periodical displacement boundary conditions guarantees the displacement continuity at the opposite surfaces between the neighboring RVEs.

By analyzing the numerical results of the model, all the stress components at the corresponding parallel boundary surfaces have the uniform stress distribution. For example, Fig. 8 shows the maximum principal stress nephogram of the whole FEM, the yarns and the resin matrix pocket in the model subjected to loading case 3. The traction continuity at the corresponding parallel boundary surfaces has been guaranteed and satisfied the periodic condition. From Fig. 8, it can be seen that the stress in yarns is about 20 times than that in the matrix pocket region. This indicates that the yarns of 3D 4-directional braided composites share the primary tensile load. As shown in Fig. 8 c, stress concentration is produced in the contacting region between the yarns and the matrix pocket. The closer to this region, the greater stress is produced.

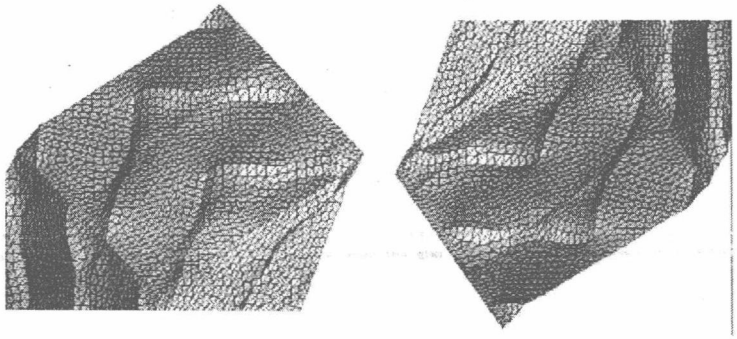

(a) Deformation of positive surface vertical to x axis

(b) Deformation of negative surface vertical to x axis

Fig. 7: Deformation of the model under loading case 6

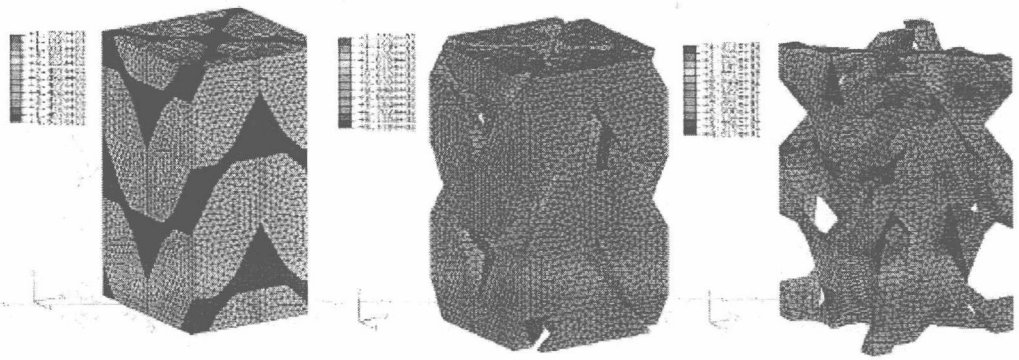

(c) Resin matrix

Fig. 8: Maximal principal stress nephogram of the model No.2 under loadind case 3

Discussion on the effective properties of 3D braided composites: The unit cell of 3D 4-directional braided composites produced by the 4-step 1×1 rectangular braiding procedures can be characterized by two independent micro-structural parameters, including the braiding angle and the fiber-volume fraction. In this section, the effects of the two parameters on the effective elastic properties of 3D braided composites are studied with the meso-mechanical FEM. The models were established as shown in this study. The width of unit cell W_x is assumed to be 2.30 mm in the models. The models with different fiber-volume fractions under a same braiding angle are obtained by defining the fiber-volume fraction of the yarn from Eq. 7. The elastic properties of fibers and matrix are shown in Table 2.

Figure 9 shows the variation of the predicted elastic constants of 3D braided composites with the increasing braiding angle, including three samples with different fiber-volume fractions. Figure 9 a describes that the elastic modulus E_z decreases sharply as the braiding angle increases. With the fiber-volume fraction increasing, the elastic modulus E_z increases as a whole. However, when the braiding angle is small, the change of the elastic modulus E_z caused by the increment of fiber-volume fraction becomes comparatively significant. Figure 9 b gives that the elastic modulus, E_x or E_y ($E_x = E_y$), varies with the braiding angle. The elastic modulus E_x increases steadily as the braiding angle increases. With the fiber-volume fraction increasing, the elastic modulus E_x increases in a similar tendency. Figure 9 c depicts that the shear modulus G_{xy} increases monotonically with the increasing braiding angle. As the fiber-volume fraction increases, the shear modulus G_{xy} increases. When the braiding angle is about 40 deg., the change of the shear modulus G_{xy} caused by the increment of the fiber-volume fraction is comparatively larger with increasing the fiber-

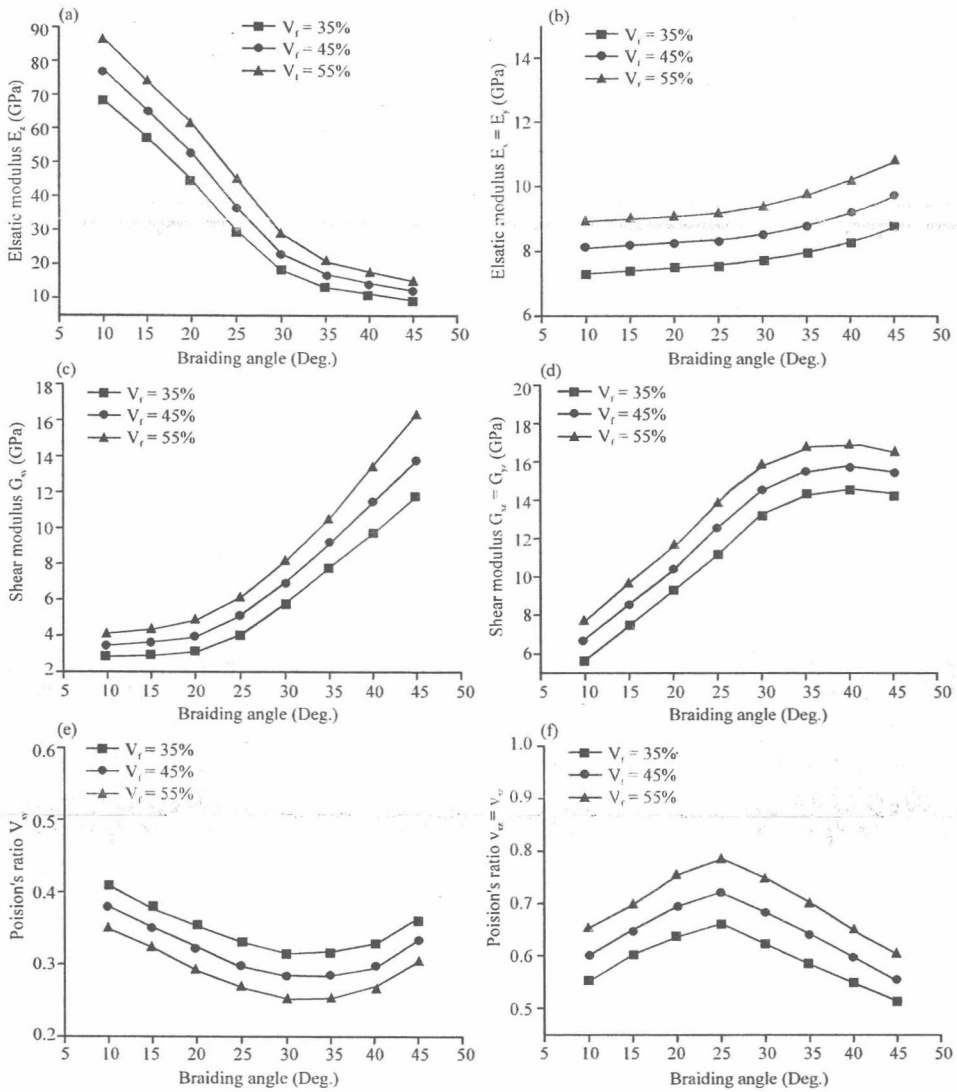

Fig. 9: Variation of engineering elastic constants with structural parameters

olume fraction. Figure 9 d presents that the shear modulus, G_{xz} or G_{yz} ($G_{xz} = G_{yz}$), firstly increases and then decreases. With the increase of the fiber-volume fraction, the shear moduli, G_{xz} and G_{yz}, increase. Figure 9 e-f shows that the variation of the Poison's ratios, v_{xy} and v_{xz} ($v_{xz} = v_{yz}$), with the braiding angle. With increasing the braiding angle, v_{xy} firstly decreases and then increases; v_{xz} and v_{yz} firstly increase and then decrease. As the fiber-volume fraction increases, the Poison's ratio v_{xy} decreases. With increasing the fiber-volume fraction, the Poison's ratios, v_{xz} and v_{yz}, increase.

As shown in Fig. 9, the effective elastic properties of the composites have been influenced by the two structural parameters. Therefore, optimization of the structural parameters can help to reduce the design time and save the manufacture costs.

CONCLUSION

A new finite element model based on the RVE is proposed to predict the effective elastic properties and the meso-mechanical behaviors of 3D braided composites. The 3D model takes into amount the periodical structure of the composites and the interaction between braiding yarns. The predicted effective elastic properties are compared favorably with the experimental data,

demonstrating the applicability of the meso-mechanical FEM. Meanwhile, the method proposed is convenient to predict the effective global stiffness of 3D braided composites. The effect of the braiding angle and fiber-volume fraction on the engineering elastic constants has been discussed in detail. The results show that the elastic modulus E_{zy} is influenced significantly by the braiding angle. By analyzing the stress distribution and deformation, it is proved that the model guarantees the displacement continuity and the traction continuity at the surface boundaries of the neighboring RVEs. The RVE-based finite element model can obtain a reasonable stress field in the meso-scale.

Future research will focus on the strength and failure analysis of 3D 4-directional braided composites by using the meso-mechanical FEM.

ACKNOWLEDGEMENT

This study is financially supported by Postgraduate Innovation Project of Jiangsu Province of China (NO. 2005065). And the authors would like to acknowledge the support given by Postgraduate Innovation Fundation of Nanjing University of Aeronautics and Astronautics (NO.BCXJ05-03).

REFERENCES

Chamis, C.C., 1989. Mechanics of Composites Materials: Past, Present and Future. J. Compos. Tech. Res., 11: 3-14.

Chen, L., Tao, X.M. and C.L. Choy, 1999. On the Microstructure of Three-Dimensional Braided Preforms. Compos. Sci. Tech., 59: 391-404.

Chen, L., X.M. Tao and C.L. Choy, 1999. Mechanical Analysis of 3-D Braided Composites by the Finite Multiphase Element Method. Compos. Sci. Tech., 59: 2383-2391.

Du, G.W. and F.K. Ko, 1993. Unit Cell Geometry of 3-D Braided Structure. J. Reinforced Plastics Compos., 12: 752-768.

Gu, B.H., 2004. Prediction of the Uniaxial Tensile Curve of 4-Step 3-Dimensional Braided Preform. Compos. Struct., 64: 235-241.

Lei, C., Y.J. Cai and F.K. Ko, 1992. Finite Element Analysis of 3-D Braided Composites, In: Advances in engineering solfware. Elsvier Sci. Pub., pp: 187-94.

Li, W., M. Hammad and S.A. El, 1990. Structural Bnalysis of 3-D Braided Preforms for Composites. J. Text Inst. 81: 491-514.

Ma, C.L., J.M. Yang and T.W. Chou, 1984. Elastic Stiffness of Three-Dimensional Braided Textile Structural Composites, Composite Materials: Testing and Design. Seven Conf., pp: 404-421.

Pandey, R. and H.T. Hahn, 1996. Visualization of Representative Volume Elements for Three-Dimensional Four-Step Braided Composites. Compos. Sci. Tech., 56: 161-170.

Sun, H.Y. and X. Qiao, 1997. Prediction of the Mechanical Properties of Three-Dimensionally Braided Composites. Compos. Sci. Tech., 57: 623-629.

Sun, H.Y., S.L. Di and N. Zhang, 2003. Micromechanics of Braided Composites via Multivariable FEM. Comput. Struct., 81: 2021-2027.

Sun, X.K. and C.J. Sun, 2004. Mechanical Properties of Three-Dimensional Braided Composites. Compos. Struct., 65: 485-492.

Tang, Z.X. and R. Postle, 2002. Mechanics of Three-Dimensional Braided Structures for Composite Materials-Part 3: Nonlinear Finite Element Deformation Analysis. Compos. Struct., 55: 307-317.

Wang, Y.Q. and A.S.D. Wang, 1994. On the Topological Yarn Structure of 3-D Rectangular and Tubular Braided Preforms. Compos Sci. Tech., 51: 575-86.

Xia, Z.H., C.W. Zhou and Q.L. Yong, 2006. On Selection of Repeated Unit Cell Model and Application of Unified Periodic Boundary Conditions in Micro-Mechanical Analysis of Composites. Int. J. Solids and Struct., 43: 266-278.

Xia, Z.H., Y.F. Zhang and F. Ellyin, 2003. A Unified Periodical Boundary Conditions for Representative Volume Elements of Composites and Applications. Int. J. Solids Struct., 40: 1907-1921.

Yang, J.M., C.L. Ma and T.W. Chou, 1986. Fiber Inclination Model of Three-Dimensional Textile Structural Composites. J. Compos Mater., 20: 472-483.

Yu, X.G. and J.Z. Cui, 2007. The prediction on mechanical properties of 4-step braided composites via two-scale method. Compos. Sci. Tech., 67: 471-480.

Zeng, T., L.Z. Wu and L.C. Guo, 2004. Mechanical Analysis of 3D Braided Composites: A Finite Element Model. Compos. Struct., 64: 399-404.

复合材料学报 第24卷 第3期 6月 2007年
Acta Materiae Compositae Sinica Vol. 24 No. 3 June 2007

文章编号：1000-3851(2007)03-0178-08

三维编织复合材料弹性性能数值预测及细观应力分析

徐 焜，许希武*
(南京航空航天大学 结构强度研究所，南京 210016)

摘 要： 基于考虑纤维束面接触的细观结构模型，引入周期性位移边界条件，采用细观有限元方法建立了材料的弹性性能预报模型。模型数值结果与试件实测数据吻合较好，证明了该模型的合理有效性。经详细分析单胞在典型工况载荷作用下的细观应力分布及变形，表明模型体现了周期性相邻单胞表面力和位移的连续性，能获得单胞更为合理的细观应力应变场。

关键词： 三维编织；复合材料；三维有限元；周期性边界条件；力学性能
中图分类号： TB332 **文献标识码：** A

Prediction of elastic constants and simulation of stress field of 3D braided composites based on the finite element method

XU Kun, XU Xiwu*
(Research Institute of Structures and Strength, Nanjing University of Aeronautics and Astronautics, Nanjing 210016, China)

Abstract: Based on the microstructure model established by the authors, coinciding with the actual configuration of braided composites, a model to predict the elastic properties was proposed by using the 3D FEM, coupled with the periodical boundary conditions. The calculated values by the model well agree with the measured values. Numerical results verify the effectiveness of the model. The stress and strain fields of the model under such typical load cases as tension and shear were analyzed in detail, respectively. The results indicate that the application of the periodical boundary conditions guarantees the continuities of the traction and displacement on the parallel boundary surfaces of the cubic model. Therefore, the stress field and the strain field obtained by the model are more reasonable than by the existing FEM models.

Keywords: 3D braiding; composites; 3D FEM; periodical boundary condition; mechanical performance

三维编织复合材料作为一种新型轻质高效结构材料，其刚度、强度等基本力学性能分析与预报是该材料用于结构设计的重要前提。但由于材料增强体为三维空间网状连续纤维结构，其细观结构极为复杂，直接建立材料力学性能预报模型困难很大。近年来，许多学者通常基于周期性单胞研究材料的基本力学行为[1]。

随着现代计算机技术和有限元理论的飞速发展，有限元方法在复合材料细观力学研究领域得到了日益广泛的应用，并已将其用于三维编织复合材料的力学建模分析，逐步建立了一批基于代表单胞的有限元分析模型。Lei 等[2]将纤维束和基体分别处理为梁元和杆元，所建模型因过分简化难以反映组分材料的受力状态；Chen 等[3]和庞宝君等[4]所建有限元刚度预报模型，因采用多相介质单元降低了建模工作量；刘振国等[5]提出了“米”字型实体单胞有限元模型，但该模型过于简单，无法体现内部纤维束的交织关系和空间构型；Sun 等[6]基于均匀化理论，采用非协调多变量有限元对比了对模量预测的影响；杨振宇等[7]所建体胞模型将纤维束截面假设为六边形，较好地体现了内部纤维束的接触特征，但建立该体胞几何模型时，忽略了表面区域细

收稿日期：2006-06-23；收修改稿日期：2006-10-08
基金项目：江苏省研究生创新计划(2005065)；南京航空航天大学博士生创新与创优基金(4003-019017)
通讯作者：许希武，教授，博士生导师，主要从事复合材料结构力学、飞行器结构完整性评定技术和计算力学研究
E-mail: xwxu@nuaa.edu.cn